# Coarsening and percolation in a disordered ferromagnet

Federico Corberi,[1,2] Leticia F. Cugliandolo,[3] Ferdinando Insalata,[1,3] and Marco Picco[3]
[1]*Dipartimento di Fisica "E. R. Caianiello," Università di Salerno, 132 Via Giovanni Paolo II, 84084 Fisciano, Salerno, Italy*
[2]*INFN, Gruppo Collegato di Salerno, and CNISM, Unità di Salerno, Università di Salerno, 132 Via Giovanni Paolo II, 84084 Fisciano, Salerno, Italy*
[3]*Laboratoire de Physique Théorique et Hautes Energies, Université Pierre et Marie Curie, Sorbonne Universités, 4 Place Jussieu, 75252 Paris Cedex 05, France*
(Received 7 November 2016; published 3 February 2017)

By studying numerically the phase-ordering kinetics of a two-dimensional ferromagnetic Ising model with quenched disorder (either random bonds or random fields) we show that a critical percolation structure forms at an early stage. This structure is then rendered more and more compact by the ensuing coarsening process. Our results are compared to the nondisordered case, where a similar phenomenon is observed, and they are interpreted within a dynamical scaling framework.

DOI: 10.1103/PhysRevE.95.022101

## I. INTRODUCTION

The phase-ordering kinetics following an abrupt change of a control parameter, like the one encountered when a magnetic system is quenched from above to below the critical temperature, is probably the simplest nonequilibrium phenomenon in which interactions among elementary constituents (spins in the previous example) drive the system from disordered configurations towards an ordered state. The main feature of such evolution is the coarsening kinetics whereby initially small domains of the different equilibrium phases compete and their typical size $R(t)$ increases in order to reduce surface tension.

Quite generally, this process is endowed with a dynamical scaling symmetry [1,2] that corresponds to the statistical self-similarity of configurations visited at different times. The only effect of the kinetics is to increase the size of the domains, preserving their morphology. Using the terminology of magnetic systems, for the equal-time spin-spin correlation function $G(r,t) = \langle s_i(t)s_j(t)\rangle$ with $r \equiv |\vec{r}_i - \vec{r}_j|$, scaling implies

$$G(r,t) = \mathcal{G}\left(\frac{r}{R(t)}\right). \tag{1}$$

This scaling form is expected to apply at distances $r$ much larger than some reference length $r_0$ that is usually associated with the lattice spacing and for times longer than some time $t_0$ that is supposed to end a nonuniversal transient regime with no scaling. Notice that, in principle, Eq. (1) should be more properly written as

$$G(r,t) = \widetilde{\mathcal{G}}\left(\frac{r}{R(t)}, \frac{L}{R(t)}\right), \tag{2}$$

where the second entry regulates the presence of finite-size effects, important when the domain sizes become similar to the system's linear dimension $L$. However, one is usually concerned with the very large system size limit $R(t) \ll L$ in which the second entry in $\widetilde{\mathcal{G}}$ diverges, $\widetilde{\mathcal{G}}(\frac{r}{R(t)}, \frac{L}{R(t)}) \simeq \widetilde{\mathcal{G}}(\frac{r}{R(t)}, \infty)$, and Eq. (1) holds with $\widetilde{\mathcal{G}}(\frac{r}{R(t)}, \infty) = \mathcal{G}(\frac{r}{R(t)})$. The scaling function $\mathcal{G}$ goes rapidly to zero for $r > R(t)$, meaning that correlations are only established up to distances comparable to the typical domain size. Regions occupied by the various phases grow similarly in the coarsening stage. Therefore, none of them prevails at any finite time if the thermodynamic limit is taken from the onset. For a magnetic system this implies that no magnetization is developed. The discussion above applies both to clean systems and to those with quenched disorder, provided randomness is sufficiently weak not to destroy the ordered phase or to introduce frustration.

It was shown in a number of papers [3–9] that, starting from a certain time $t_p$, some geometrical features of the growing domains in a clean two-dimensional coarsening spin system are very accurately described by the well-known properties of critical percolation [10–12] at the critical threshold $p_c$, where a fractal spanning or wrapping cluster exists. This fact comes as a surprise, since percolation is a paradigm of a noninteracting problem, whereas coarsening embodies exactly the opposite. However, although apparently paradoxical, the interactions among the spins provide the mechanism whereby percolative features are built at times of order $t_p$. Indeed, since the initial state is uncorrelated, it is an instance of random percolation and the absence of magnetization sets the concentration of up and down spins to $1/2$. Clusters in such a state, therefore, are too thin to extend across the entire system, because $1/2 < p_c \simeq 0.59$ on the square lattice typically used in a simulation. Hence, the formation of a spanning or wrapping object at $t_p$ is certainly an effect of the ordering kinetics. Quite intriguingly, in fact, as correlations stretch to larger and larger distances, the droplet structure manages to connect initially disjoint parts until the largest domain crosses the entire system and acquires the geometric properties of the percolation cluster at threshold. If $t \geqslant t_p$ such a domain is surely stable and persists up to the longest times (although, obviously, some of its geometrical features change in time, as we will discuss further). This is indeed how $t_p$ is defined.

From $t = t_p$ onward, phase ordering exhibits the fractal properties of uncorrelated critical percolation on sufficiently large scales. As a matter of fact, since the magnetization remains zero at all times, such properties occur in a correlated system with $p = 1/2 < p_c$. These two apparently contradicting instances, uncorrelated percolation akin to the one occurring at $p = p_c$ on the one hand and correlated coarsening with $p = 1/2$ on the other, can be actually reconciled because they occur on well-separated distances. Percolative properties

 

are confined on length scales $r \gg R(t)$ larger than those where, due to the interactions, some correlation has already developed. Instead, on length scales $r < R(t)$, where the interactions are at work, the correlations compactify the fractal domains and the percolative geometry is lost. Interactions therefore play the two contrasting roles of promoting the formation of the critical percolation cluster and progressively destroying it at scales of order $R(t)$.

This framework is quite clearly exhibited in the clean (i.e., nondisordered) two-dimensional kinetic Ising model with single spin-flip dynamics for which $t_p$ is shown to scale with the system size $L$ as [9]

$$t_p \propto L^{z_p}, \tag{3}$$

where $z_p$ is a new dynamical exponent that depends on the properties of the lattice populated by the spins and is typically smaller than 2. This relation suggests the introduction of a growing length associated with the approach to critical percolation

$$R_p(t) \simeq t^{1/z_p} \tag{4}$$

that saturates, reaching the linear system size $L$ at $t = t_p$, namely, $R_p(t_p) = L$. Furthermore, for such nonconserved scalar order parameter dynamics, $R(t) \simeq t^{1/z_d}$ with $z_d = 2$ quite generally. Then

$$R_p(t) \simeq (t^{1/z_d})^{z_d/z_p} \simeq [R(t)]^{z_d/z_p}. \tag{5}$$

On the basis of extensive numerical simulations, it was conjectured in [9] that $z_d/z_p = n$, the coordination of the lattice, for this kind of dynamic rule. Other clean systems evolving with different microscopic rules (local and nonlocal spin exchange and voter) on various lattices are treated in [13] and more details are given in this paper, where the guess $R_p(t) \simeq [R(t)]^n$ is revisited. Here we use Glauber dynamics, which we define below. Notice that $R_p(t_p) = L$ implies

$$R(t_p) = L^{z_p/z_d}. \tag{6}$$

Interestingly, the existence of a percolating structure in coarsening systems is at the heart of one of the few analytical results in finite-dimensional phase ordering in two dimensions [3,4]. In fact, the distribution of cluster areas in percolation is exactly known [14] and, since the evolution of a single hull-enclosed area in a nonconserved scalar order parameter dynamics can be inferred, an exact expression for the area distribution at any time in the scaling regime can be derived, building upon the one at random percolation.

As mentioned above, the relevance of percolation in phase-ordering kinetics was initially addressed in a homogeneous system without quenched disorder. Real systems, on the other hand, are seldom homogeneous, due to the occurrence of lattice defects, because of position-dependent external disturbances, or for other reasons. This fact deeply perturbs the scaling properties [15]. Indeed, although some kind of symmetry comparable to Eq. (1) is reported in some experiments [16,17], the asymptotic growth law $R(t)$ is much slower than in a clean system [16–20]. Similar conclusions are reached in the numerical studies of models of disordered ferromagnets, such as the kinetic Ising model in the presence of random external fields [21–32], with varying coupling constants [32–39], or in the presence of dilution [33,38,40–47].

A natural question is then whether the percolation effects observed in two-dimensional clean systems show up also in the disordered ones. The answer is not pat because our knowledge in this field is still rather scarce. Even simple questions regarding the nature of the dynamical scaling or the form of the growth law $R(t)$ remain largely unanswered in the presence of disorder. In [48] the geometric properties of the domain areas in a coarsening Ising model with weak quenched disorder were studied, but the analysis of the time needed to reach the critical percolation structure and the detailed evolution during the approach to this state were not analyzed. In this article we settle this issue. By means of extensive numerical simulations of the kinetics of the random field Ising model (RFIM) and the random bond Ising model (RBIM), we show the existence of a spanning cluster with the geometry of critical percolation starting from a certain time $t_p$. This feature is akin to what was observed in clean systems. Moreover, other quantitative properties such as the size dependence (3) of the characteristic time $t_p$ and many other details turn out to be reproduced in the presence of disorder. This fact qualifies the relation between coarsening and percolation as a robust phenomenon, the origin of which is deeply rooted in the physics of order-disorder transitions in two dimensions. Besides being interesting and informative on their own, the results of this paper also represent a step towards a theory of phase ordering in two-dimensional disordered ferromagnets, in the same spirit as the one developed in [3,4] for clean systems. Needless to say, this would represent an important achievement in such a largely unsettled field.

This paper is organized as follows. In Sec. II we introduce the model that will be considered throughout the paper and the basic observables that will be computed. In Sec. III we discuss the outcome of our simulations, for both the clean case (Sec. III A) and the disordered ones (Sec. III B). We conclude the paper in Sec. IV by summarizing the results and discussing some issues that remain open.

## II. MODEL AND OBSERVABLE QUANTITIES

We will consider a ferromagnetic system described by the Hamiltonian

$$\mathcal{H}(\{S_i\}) = -\sum_{\langle ij \rangle} J_{ij} S_i S_j + \sum_i H_i S_i, \tag{7}$$

where $S_i = \pm 1$ are Ising spin variables defined on a two-dimensional $L \times L$ square lattice (different lattices were considered in [13]) and $\langle ij \rangle$ are two nearest-neighbor sites. The properties of the coupling constants $J_{ij}$ and the external field $H_i$, specified below, define the two disordered models that will be studied in this paper. In the RBIM $H_i \equiv 0$ and the coupling constants are $J_{ij} = J_0 + \delta_{ij}$, where $\delta_{ij}$ are independent random numbers extracted from a flat distribution in $[-\delta, +\delta]$, with $\delta < J_0$ in order to keep the interactions ferromagnetic and avoid frustration effects. In the RFIM the ferromagnetic bonds are fixed $J_{ij} \equiv J_0$ (i.e., $\delta_{ij} \equiv 0$), while the external field $H_i = \pm h$ is uncorrelated in space and sampled from a symmetric bimodal distribution.

The ordered state, typical of the clean system below the critical temperature $T_c$, is preserved in the RBIM because the randomness of the coupling constants is constrained to

keep them all ferromagnetic. Something else occurs in the RFIM, because the external fields efficiently contrast the ordering tendency down to $T = 0$ in any $d \leqslant 2$. This is easily explained by the Imry-Ma argument [49], which, upon comparing the energy increase $\Delta E_{\rm surf} \propto J_0 \ell^{d-1}$, due to the reversal of a bubble of size $\ell$ in an ordered phase, to its decrease $\Delta E_{\rm field} \propto h \ell^{d/2}$, due to the possible alignment of its spins with the majority of the random fields, shows the existence of a threshold length

$$\ell_{\rm IM} \sim \left(\frac{h}{J_0}\right)^{2/(d-2)} \tag{8}$$

above which flipping droplets becomes favorable, thus disordering the system for $d \leqslant 2$ (it can be shown that ordering is suppressed also right at $d = 2$). Moreover, still for $d < 2$, $\ell_{\rm IM} \to \infty$ as $\frac{h}{J_0} \to 0$ so that, if such a limit is taken from the onset, the system orders in any dimension, even down to $d = 1$ [23]. In the following, as we will discuss further below, we will consider this limit.

Dynamics can be introduced in the Ising model with Hamiltonian (7) by flipping single spins according to the Glauber transition rates at temperature $T$,

$$w(S_i \to -S_i) = \frac{1}{2}\left[1 - S_i \tanh\left(\frac{H_i^W + H_i}{T}\right)\right], \tag{9}$$

where the local Weiss field

$$\begin{aligned} H_i^W &= \sum_{j\in\mathcal{N}(i)} J_{ij} S_j = J_0 \sum_{j\in\mathcal{N}(i)} S_j + \sum_{j\in\mathcal{N}(i)} \delta_{ij} S_j \\ &= H_{i,\rm det}^W + H_{i,\rm rand}^W \end{aligned} \tag{10}$$

is decomposed, for the RBIM, into a deterministic and a random part [the sum runs over the nearest neighbors $\mathcal{N}(i)$ of $i$].

The quenching protocol amounts to evolving a system prepared at time $t = 0$ in an uncorrelated state with zero magnetization (representing an equilibrium configuration at $T = \infty$) with spin flips regulated by the transition rates (9) evaluated at the final temperature $T = T_f$. In this paper we focus on the limit $T_f \to 0$ while keeping the ratio $\epsilon = \frac{\delta}{T_f}$ (for the RBIM) or $\epsilon = \frac{h}{T_f}$ (for the RFIM) finite. We will also set $J_0 = 1$. The discussion below Eq. (8) points out that in this limit $\ell_{\rm IM} \to \infty$ and phase ordering always occurs also in the RFIM. Moreover, the transition rates (9) take the simple form

$$w(S_i \to -S_i) = \begin{cases} 1 & \text{for} \quad H_{i,\rm det}^W S_i < 0 \\ 0 & \text{for} \quad H_{i,\rm det}^W S_i > 0 \\ \frac{1}{2}\left[1 - S_i \tanh\left(\frac{H_{i,\rm rand}^W + H_i}{T}\right)\right] & \text{for} \quad H_{i,\rm det}^W S_i = 0, \end{cases} \tag{11}$$

which shows that the model depends only on the ratio $\epsilon$. Having a theory with a single parameter is only one of the advantages of the limit we are considering. The low-temperature limit also reduces the thermal noise and allows for an accelerated updating rule, since Eq. (11) shows that only spins with $H_{i,\rm det}^W \leqslant 0$ need to be updated. These are basically the spins on the corners of interfaces, a small fraction of the total number of spins in the sample, especially at long times.

We have computed the average size of the domains $R(t)$ as the inverse density of defects [1], namely, by dividing the number $L^2$ of lattice sites by the number of spins that are not aligned with all the neighbors. An ensemble average is then performed.

The equal-time pair correlation function, which was defined above Eq. (1), is computed as

$$G(r,t) = \frac{1}{4L^2} \sum_i \sum_{i_r} \langle S_i S_{i_r} \rangle, \tag{12}$$

where the spins are measured at time $t$, the $i_r$'s are the four sites at distance $r$ from $i$ along the horizontal and vertical directions, and $\langle \cdots \rangle$ represents a nonequilibrium ensemble average that is taken over different realizations of the initial configuration and over various thermal histories, namely, the outcome of the probabilistic updates of the spins. We adopt periodic boundary conditions, so $i_r$ in Eq. (12) is to be intended modulo $L$.

As explained in Sec. I, assuming that $R(t) \ll L$, the two-parameter scaling form (2) transforms into the more conventional single-parameter one in Eq. (1). However, Eq. (5) shows that another growing length $R_p(t)$ is on the scene. The fact that $z_p < z_d$ implies that this length grows faster than $R(t)$. Therefore, given a finite size $L$ of the system, $R_p(t)$ may become of the order of $L$ even if the condition $R(t) \ll L$, which is usually considered the hallmark of a finite-size free situation, is met. In this case, a simple scaling form like the one in Eq. (1) must be upgraded to a form akin to Eq. (2) (with $R_p$ playing the role of $R$ in the second entry) in order to take into account the two characteristic lengths. Indeed, it was shown in [9] that a two-parameter scaling

$$G(r,t) = g\left(\frac{r}{R(t)}, \frac{L}{R_p(t)}\right) \tag{13}$$

is more appropriate to describe the space-time correlation data.

The correlation function (12) is shown in Fig. 1 for the clean model quenched to $T_f = 0$ (more simulation details are given in Sec. III). The simple scaling form in Eq. (1) would imply the collapse of the curves relative to different values of $R(t)$ in this kind of plot. Instead, there is a systematic deviation of the curves at large $r$ as $R(t)$ increases. As anticipated, this is because the correct scaling form is Eq. (13) instead of Eq. (1). With a two-parameter scaling as in Eq. (13), plotting against $r/R(t)$ only fixes the first entry, namely, $r/R(t)$, but the second one, namely, $L/R_p(t)$, still changes as time elapses. This produces the failure of the collapse observed in Fig. 1. In order to superimpose the curves one should also keep the second entry fixed. This can only be done by using a different system size $L$ for each different value of $R_p(t)$. It was shown in [9] that in so doing one obtains an excellent scaling in the clean system. This confirms the validity of the form (13).

An important quantity to assess percolation properties is the pair connectedness function. In percolation theory this quantity is defined as the probability that two points separated by a distance $r$ belong to the same cluster. In two dimensions, random percolation theory at $p = p_c$ gives [10–12]

$$C_{\rm perc}(r, r_0) \sim \left(\frac{r}{r_0}\right)^{-2\Delta}, \tag{14}$$

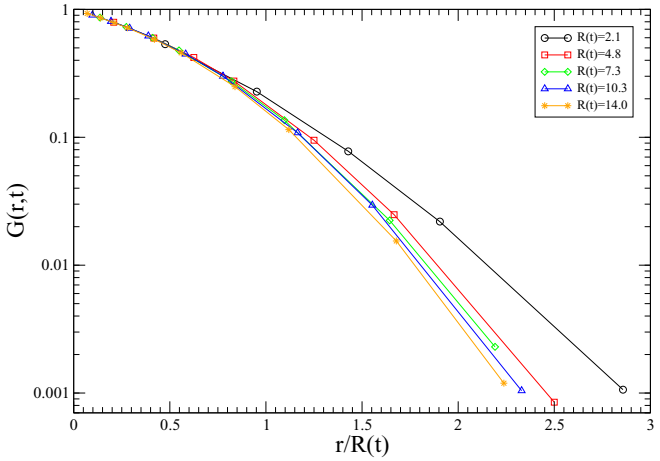


FIG. 1. Spin-spin correlation function $G(r,t)$ against $r/R(t)$ on a log-linear scale for a quench of the clean Ising model to $T_f = 0$. Different curves correspond to different values of $R(t)$ (see the key), namely, of time $t$. The system size is $L = 512$. The deviations from collapse at large values of the scaling variable $r/R(t)$ are ascribed to the effects of the approach to critical percolation that has to be taken into account with a second scaling variable. See the text for the explanation of this fact.

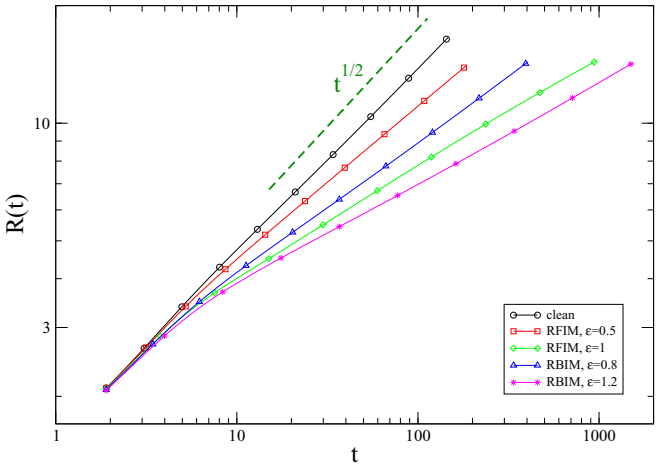


FIG. 2. Growing length $R(t)$ plotted against time on a log-log scale for the different models considered in this paper and for different values of the disorder strength $\epsilon$ (see the key). The dashed green line is the asymptotic behavior $t^{1/2}$ expected for the clean case.

where $r_0$ is a reference distance, usually the lattice spacing. Equation (14) holds true for large $r/r_0$, with the critical exponent $\Delta = 5/48$. The dotted black curve in Fig. 4 is a numerical evaluation of $C_{\rm perc}$ on a square lattice with $r_0 = 1$ and $L = 512$. The curve is indistinguishable from Eq. (14) except at large distances, where finite-size effects set in.

In the coarsening system we evaluate the pair connectedness correlation as follows: At a given time, after identifying all the domains of positive and negative spins, the connectivity is computed as

$$C(r,t) = \frac{1}{4L^2} \sum_i \sum_{i_r} \langle \delta_{S_i,S_{i_r}} \rangle, \tag{15}$$

where $\delta_{S_i,S_j} = 1$ if the two spins belong to the same cluster, namely, they are aligned and there is a path of aligned spins connecting them, and $\delta_{S_i,S_j} = 0$ otherwise.

Another quantity that will be considered is the (average) squared winding angle $\langle \theta^2 \rangle$. Its definition is the following: At a given time, we choose two points $i, j$ on the external perimeter (the hull) of a cluster and we compute the winding angle $\theta_{ij}$, namely, the angle (measured counterclockwise) between the tangent the angle (measured counterclockwise) between the tangents to the perimeter at sites $i$ and $j$. After repeating the procedure for all the couples of perimeter points at distance $r$ (measured along the hull), taking the square and averaging over the nonequilibrium ensemble, $\langle \theta^2(r) \rangle$ is obtained. The behavior of $\langle \theta^2(r) \rangle$ is exactly known in two-dimensional critical percolation at $p = p_c$ [50,51], where one has

$$\left\langle \theta^2_{\rm perc}(r,r_0) \right\rangle = a + \frac{4k}{8+k} \ln\left(\frac{r}{r_0}\right), \tag{16}$$

with $k = 6$ and $a$ a nonuniversal constant. We will compute this same quantity in the coarsening systems upon moving along the hulls of the growing domains (in this case, we will only consider the largest cluster for numerical convenience).

## III. NUMERICAL RESULTS

In this section we present the results of our numerical simulations of the kinetic Ising model. We start with a study of the clean system in Sec. III A. Although some percolation effects have already been reported for clean systems [3–9], in this section we introduce different tools, such as the connectivity (15) and the winding angle (16). This case therefore serves not only to compare with the disordered systems considered later, but also as a benchmark for these quantities.

We will then turn to the behavior of the disordered models in Sec. III B. Let us remark that the very slow growth of $R(t)$ in such systems as compared to the clean case (see Fig. 2) introduces severe limitations on the range of values of $R(t)$ than can be accessed. Moreover, large system sizes imply large values of $t_p$ [see Eq. (3)], making the regime in which the percolation structure has been fully established, $t \gg t_p$ or, equivalently, $R_p(t) \gg L$, inaccessible numerically. For this reason we will work with moderate values of $L$. In order to compare the dynamics of the clean systems to that of the disordered ones under similar conditions, the same choice will be made for the pure system.

All the results contained in this section are obtained with periodic boundary conditions by averaging over a nonequilibrium ensemble with order $10^5$–$10^6$ realizations. The system linear size is $L = 512$ in units of the lattice spacing.

### A. Clean case

Let us consider a quench of the clean Ising model to $T_f = 0$. The wrapping cluster that develops at $t \simeq t_p$ can cross the system in different ways. The first possibility is to span the system from one side to the other horizontally or vertically. We denote the probabilities of such configurations by $\pi_{1,0}$ and $\pi_{0,1}$, respectively. Obviously, for a lattice with unit aspect ratio,

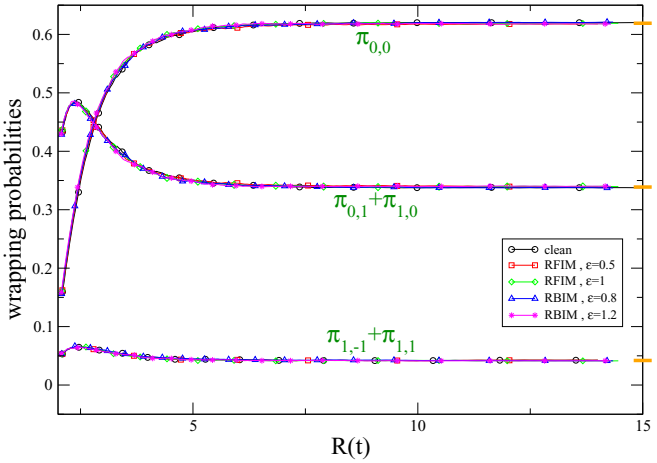


FIG. 3. Three wrapping probabilities $\pi_{0,0}$, $\pi_{0,1}+\pi_{1,0}$, and $\pi_{1,-1}+\pi_{1,1}$ plotted against $R(t)$ for a square lattice system with linear size $L = 512$. Each set of superimposing curves represents one of these quantities (as labeled in the figure) for different values of the disorder strength (see the key), including the clean case. The exact values of random percolation are marked with a bold (orange) segment on the extreme right.

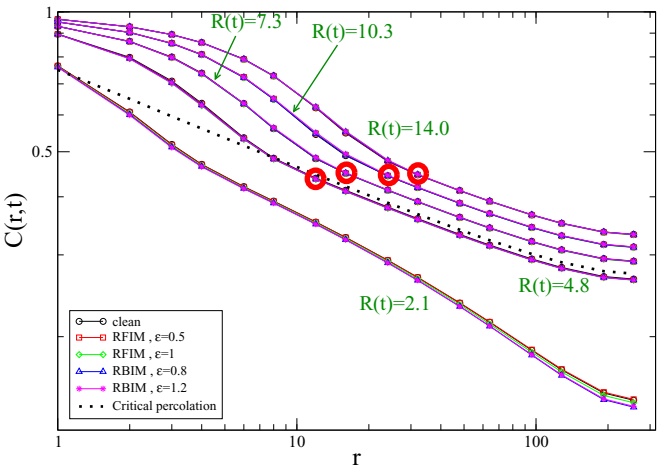


FIG. 4. Connectedness $C(r,t)$ plotted against $r$. Each set of superimposing curves represents this quantity for a given value of $R(t)$ [$R(t) = 2.1,4.8,7.3,10.3,14.0$, from bottom to top, as indicated in the figure] for different values of the disorder strength (see the key), including the clean case (black curves with circles). The same quantity computed numerically in a random percolation square lattice at $p = p_c$ is represented by the dotted black curve, which agrees with the exact form (14) apart from some finite-size effects at large $r$. The red circles correspond to the point where the percolative behavior starts to be observed.

$\pi_{0,1} = \pi_{1,0}$. Another possibility is to have a domain traversing the sample in both the horizontal and the vertical directions, the probability of which we indicate by $\pi_{0,0}$. Finally, clusters can percolate along one of the two diagonal directions with equal probabilities $\pi_{1,-1}$ and $\pi_{-1,1}$. Since we operate with periodic boundary conditions, other wrapping shapes, winding the torus more than once, are also possible, but these will not be considered in the following since they occur with an extremely small probability. The quantities mentioned above are exactly known for two-dimensional critical percolation under periodic boundary conditions. They are [52]

$$\begin{aligned} \pi_{0,1} + \pi_{1,0} &\simeq 0.3388, \\ \pi_{0,0} &\simeq 0.619\,08, \\ \pi_{1,-1} + \pi_{1,1} &\simeq 0.041\,96. \end{aligned} \tag{17}$$

The wrapping probabilities during the phase-ordering process are plotted against $R(t)$ (shown in Fig. 2) in Fig. 3. The black curves with circles, which are perfectly superimposed on the others, represent the clean case at hand.

The wrapping probabilities start from zero immediately after the quench since there cannot be any crossing in the initial state. A first observation is that they saturate at long times [large $R(t)$] to values that are very precisely consistent with the values at critical percolation given in Eq. (17) (bold orange segment on the far right). This fact was first pointed out in [6,7]. The second observation is that all these probabilities attain their asymptotic values around a certain $R(t)$ that can be used as a rough estimation of $R(t_p)$. Concretely, it occurs at $R(t) \gtrsim 5$ for $L = 512$. Repeating the numerical experiment in systems with different sizes, indeed, one can check that this determination of $R(t_p)$ increases with $L$, as it is expected after Eq. (5).

The next quantity we consider is the pair connectedness defined in Eq. (15). In Fig. 4 we plot this quantity against $r$ for different values of $R(t)$, namely, of time measured with the relevant clock (black curves with circles, which are perfectly superimposed on the others, represent the clean case at hand). The area $S(t) = \sum_r C(r,t)$ below the curves increases as time elapses, because $S(t)$ is the probability that two points chosen at random belong to the same cluster and the number of domains decreases during coarsening. Regarding the form of each curve, after a first transient that we identify as $t \lesssim t_p$, the typical power-law behavior of critical percolation, Eq. (14) (dotted black line) is observed. This, however, is only true for values of $r$ larger than a certain time-dependent value. This can be explained as due to the fact that on scales smaller than $R(t)$ correlations set in and domains become compact. It is therefore natural to observe the percolative behavior only at distances larger than $R(t)$.

Let us now discuss the quantitative properties of the pair connectivity $C$, in particular, its scaling behavior. According to the discussion around Eq. (13), we expect a two-parameter scaling, namely,

$$C(r,t) = c\left(\frac{r}{R(t)}, \frac{L}{R_p(t)}\right), \tag{18}$$

where $c$ is a scaling function. In order to make the presentation simpler, let us start by discussing the scaling properties for times that are much longer than the one $t_p$ when the percolating structure sets in. In this limit, the second entry in Eq. (18) is small and one has

$$C(r,t) \simeq c\left(\frac{r}{R(t)}, 0\right) = \mathcal{C}\left(\frac{r}{R(t)}\right), \tag{19}$$

where $\mathcal{C}$ is a single-variable scaling function. One can infer the form of the scaling function $\mathcal{C}(x)$ for large values of $x$ as follows. After $t_p$ the system has percolative properties for $r > R(t)$ and it can be thought of as a percolation problem on

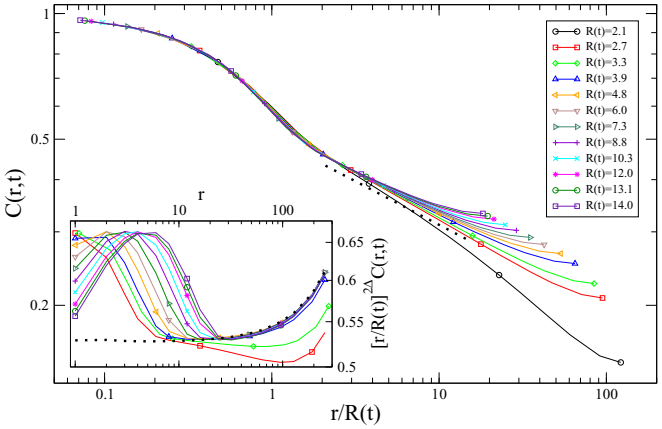


FIG. 5. Connectedness $C(r,t)$ against $r/R(t)$ in the clean case, for different values of $R(t)$ (see the key) showing conventional scaling for short lengths compared to $R(t)$. The dotted black line is the behavior (21). In the inset, $[r/R(t)]^{2\Delta}C(r,t)$ is plotted against $r$. The dotted black line is the same curve as in Fig. 4, namely, the connectedness function computed numerically in a random percolation square lattice at $p = p_c$. The curves fail to scale on short lengths now but the plot demonstrates that the long lengths behave as in critical percolation.

a lattice with spacing $R(t)$, for which Eq. (14) must hold with the replacement $r_0 \to R(t)$. Thus,

$$C(r,t) \sim \left(\frac{r}{R(t)}\right)^{-2\Delta} \quad \text{for} \quad r \gg R(t). \tag{20}$$

In order to match Eqs. (19) and (20) in the long-distance limit $r \gg R(t)$, one needs

$$\mathcal{C}(x) \simeq x^{-2\Delta} \quad \text{for} \quad x \gg 1. \tag{21}$$

In the opposite short-distance limit $r \ll R(t)$, we are exploring the properties of the domains well inside their correlated region, where there is no percolative structure and the scaling function $c$ decays faster. All the above holds for $t \gg t_p$ where the second entry in the scaling function in Eq. (18) is very small. In the opposite situation $t \ll t_p$ (but $t$ larger than the microscopic time $t_0$ when scaling sets in) one has

$$C(r,t) \simeq c\left(\frac{r}{R(t)}, \infty\right) = \Xi\left(\frac{r}{R(t)}\right). \tag{22}$$

For $r \gg R(t)$ the scaling function $\Xi$ is expected to be different from $\mathcal{C}$, because these two functions describe two contrasting situations in which the percolative structure is absent or present, respectively. For $r \ll R(t)$, instead, the scaling function $\Xi$ should be akin to $\mathcal{C}$, because in any case the domain structure is shaped by correlations on these short length scales.

Let us submit these scaling ideas to the numerical test. In Fig. 5 we plot $C(r,t)$ against $r/R(t)$. Let us discuss the behavior at $t \gg t_p$ and $t \ll t_p$ separately.

We start by discussing the regime of sufficiently long times $t \gg t_p$. Considering the previous rough estimate $R(t_p) \gtrsim 5$ obtained from the inspection of the wrapping probabilities (see Fig. 3), we can assume that such a regime can be sufficiently well represented by the curves with $R(t) \geqslant 4.8$ in Fig. 5. According to Eq. (18), we should find collapse at different times on a unique master curve $\mathcal{C}$, with the behavior (21). The numerical data show superposition, except in a region of large $r$ (which moves towards smaller values of $r$ as time elapses) where data collapse is lost due to finite-size effects. Notice also that, from $x \gtrsim x_{\rm perc} = 1.6$, the master curve behaves as in Eq. (21), as can be checked by comparing the numerical data with the dotted black line. The departure from the behavior (21) at very large $x$ is always flanked by the failure of data collapse, a fact that strengthens the idea that these effects are due to finite-size corrections. In the inset in the same figure we plot $[r/R(t)]^{2\Delta}C(r,t)$ against $r$ for all data in the main panel except those for $R(t) = 2.1$. The data collapse onto a master curve that is flat at not so large $r$ and then bends upward due to finite-size corrections. The latter can be captured by a correcting factor $f(r/L)$ to be added as a factor to the scaling law (20). In the inset we also show the data for actual critical percolation that are superimposed on the dynamic data, thus confirming that the bending of the curves is not a dynamic effect but just conventional finite-size corrections.

We now move to the regime with $t \ll t_p$. The curves with $R(t) = 2.1$ and $R = 2.7$ in Fig. 5 are representative of such a regime. We find that these two lines do not collapse for all values of $x > x_{\rm perc}$. This is because for relatively small values of $L$ the regime with $R(t) \ll L$ where Eq. (22) holds is not fully reached in our simulations. However, it is interesting to observe that in the region $x < x_{\rm perc}$ data collapse is obeyed on a master curve $\Xi$ that is almost indistinguishable from $\mathcal{C}$, as expected according to the discussion below Eq. (22). On the other hand, in the region $x > x_{\rm perc}$ a marked difference is observed between the curves with $R \leqslant 2.7$ and those with $R(t) \geqslant 4.8$. This is due to the fact that the percolative structure is still absent when the former ones are computed while it is established in the later measurement.

Finally, let us comment on the fact that the quantity $C$, besides being very informative about the twofold properties of the system (compact and correlated at small distances vs fractal and uncorrelated at large distances), is also very well suited to assess the role of the *extra* growing length $R_p(t)$ in determining the scaling properties. Indeed, although in [9] indications that Eq. (13) reproduces the data for $G$ better than the simple form (1) were given, the deviations from Eq. (1) were relatively small and located in the region of large $r$ where $G$ becomes very small. Instead, as Fig. 5 clearly shows, a single-variable scaling form for $C$ completely fails in describing the data, due to the differences between $\mathcal{C}$ and $\Xi$ in the region $x > x_{\rm perc}$. For this quantity the improvement of Eq. (18) over a single parameter scaling is conspicuous.

The last quantity that we will consider is the winding angle, which is plotted in Fig. 6 (the clean case corresponds to the black lines with circles, which are perfectly superimposed on the others) for various choices of $R(t)$. Following the discussion about the connectivity, for $t > t_p$ we expect to observe the percolative behavior of Eq. (16), with the replacement $r_0 \to R(t)$. In other words [50,51],

$$\langle \theta^2(r,t) \rangle = a + \frac{4k}{8+k} \ln\left(\frac{r}{R(t)}\right) \tag{23}$$

for $r \gg R(t)$. If this is true we ought to find data collapse of the curves for $\langle \theta^2(r,t) \rangle$ at different times when plotted against $r/R(t)$, if $r \gg R(t)$ is large enough and $R(t) \gg R(t_p)$ [similarly to what was previously observed for $C(r,t)$ (see

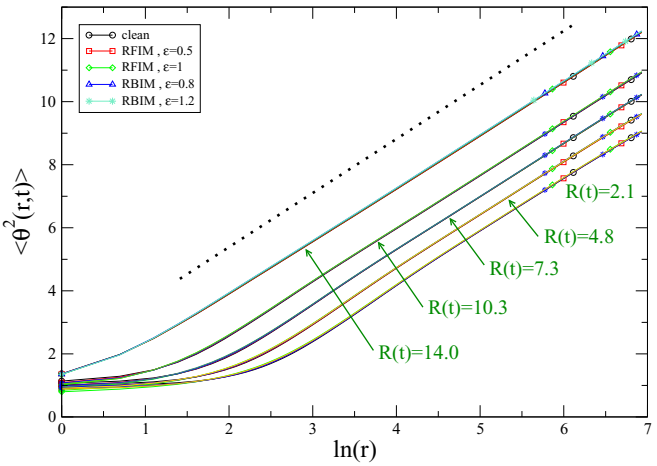


FIG. 6. Winding angle $\langle\theta^2(r,t)\rangle$ plotted against $\ln r$. Each set of superimposing curves represents this quantity for different values of the disorder strength (see the key), including the clean case. The exact form (16) of random percolation is the dotted black curve (the constant $a$ is arbitrarily fixed to be $a = 2$).

Fig. 5)]. In addition, the master curve should be the one of Eq. (23) for $r$ sufficiently larger than $R(t)$. This kind of plot is shown in Fig. 7. Interestingly, not only do we observe data collapse on the master curve (23) when $t \gg t_p$, but this occurs with good precision also for a value $R(t) = 2.1$, which was shown in Fig. 5 to be representative of a situation with $t < t_p$. This implies that, for this particular quantity, a single-parameter scaling

$$\langle\theta^2(r,t)\rangle = \mathcal{T}\left(\frac{r}{R(t)}\right), \tag{24}$$

where $\mathcal{T}(x)$ is a scaling function, accounts for the data. This does not contradict the general fact that, due to the existence of the extra length $R_p$, a two-parameter scaling has to be expected. Indeed, Eq. (24) is a particular case of

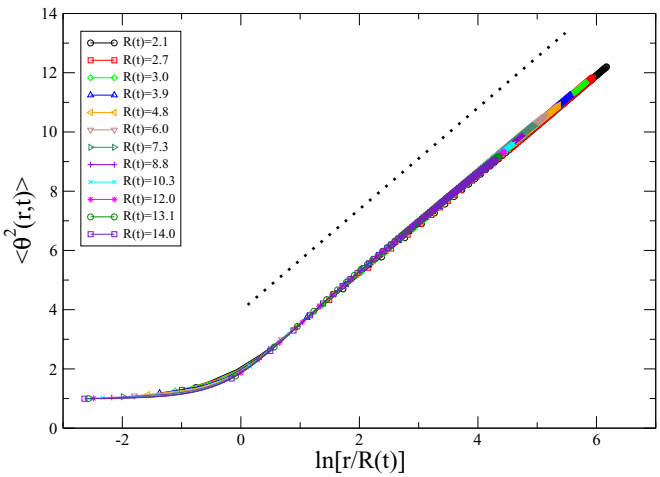


FIG. 7. Winding angle $\langle\theta^2(r,t)\rangle$ plotted against $\ln[r/R(t)]$ for the pure case. The exact form (16) of random percolation is the dotted black curve (the constant $a$ is arbitrarily fixed to be $a = 4$).

a two-parameter form

$$\langle\theta^2(r,t)\rangle = \Theta^2\left(\frac{r}{R(t)}, \frac{L}{R_p(t)}\right), \tag{25}$$

where $\Theta^2$ is a scaling function with a weak dependence on the second entry.

### B. Quenched disorder

In this section we discuss the effects of quenched disorder on the approach to percolation by considering the dynamics of the RFIM and the RBIM. We investigate the properties of the same quantities analyzed in the clean limit in Sec. III A.

Before starting this analysis let us briefly overview what is known about the coarsening behavior of weakly disordered models. When weak disorder is added, the growth law $R(t)$ is markedly slowed down with respect to its behavior in the pure case. This is observed in the RFIM and in the RBIM as well. In particular, in the low-temperature limit we are considering in this paper, i.e., $T \to 0$ with fixed $\epsilon$ [see the discussion around Eq. (11)], a regime with an effective algebraic law $R(t) \sim t^{1/\zeta(\epsilon)}$ is entered after a microscopic time. The effective growth exponent, starting from the value $\zeta(\epsilon = 0) = 2$ of the clean case, monotonically increases with $\epsilon$ [33,53]. This shows that in this stage $R(t)$ grows slower in the disordered models than in the clean case. All these features can be quite neatly observed in Fig. 2, where the behavior of $R(t)$ is shown. At rather long times, there is a crossover at $t_{\rm cross}$ to an even slower growth, with $R(t)$ increasing logarithmically, representing the asymptotic behavior [53,54]. The simulations presented in this paper will never enter such an asymptotic stage; they will be restricted to $t < t_{\rm cross}$.

The slowing down of $R(t)$ reflects a fundamental difference in the coarsening mechanisms at $\epsilon = 0$ and $\epsilon \neq 0$. In the clean system phase ordering proceeds by softening and flattening of interfaces, which is promoted by surface tension and is a nonthermal effect. This means that activated processes are irrelevant and, as a consequence, the kinetics has the same basic features at any $T_f < T_c$, including $T_f = 0$ (which is indeed the case presented in the previous section). On the other hand, as soon as some disorder (no matter how weak) is present, interfaces get stuck in pinned configurations and the evolution can only be promoted by thermal activation. These systems are frozen at $T_f = 0$ (this is why we work at finite, although vanishingly small, temperatures $T_f \to 0$).

The main result of this section is that, although $R(t)$ increases in a radically different way and the dynamics in the presence of disorder is fundamentally different from that of the pure case, the percolative features observed in the clean case occur with the same qualitative and quantitative modality in the presence of disorder. Moreover, this occurs for both random fields and random bonds.

In order to prove the statement in the preceding paragraph, let us start by discussing the behavior of the crossing probabilities introduced at the beginning of Sec. III A. These quantities are plotted in Fig. 3. For both the RFIM and the RBIM and for any strength of disorder parametrized by $\epsilon$, these probabilities are indistinguishable from those of the clean $\epsilon = 0$ case. This shows that the effect of disorder does not spoil the occurrence of the percolative structure or how and when [provided time is

parametrized in terms of $R(t)$] it is formed. As a by-product, the independence of the crossing probabilities of $\epsilon$ implies that Eq. (6) is valid beyond the pure case, with a unique value of the exponent $z_p/z_d$, at least for the nonconserved order parameter dynamics on the square lattice considered here. Let us mention that, since $R(t)$ is strongly $\epsilon$ dependent, we should not find the nice collapse of Fig. 3 if we plotted against time, instead of against $R(t)$. Equation (6) would not look $\epsilon$ independent upon expressing $R_p$ as a function of time either, namely, in the form of Eq. (3). This shows that the typical size of correlated domains is the natural parametrization of time in this problem. It will also help us reach a conclusion about the system size dependence of the percolation time $t_p$ without having to simulate different system sizes, as we will explain below.

Let us move on to the connectedness function. A comparison between the clean case and the disordered ones is presented in Fig. 4. In this figure one sees that all the disordered cases fall onto the clean case provided times are chosen in order to have the same growing length. For instance, the curve for $t = 103$ without disorder is indistinguishable from that at $t = 1446$ for the RBIM with $\epsilon = 1.2$, because at these times the size $R(t)$ of the domains in the two models is the same, $R(t) = 14.0$ (the topmost curve in Fig. 4). Notice that collapse of the various curves is obtained for the RFIM and the RBIM and for any strength $\epsilon$ of disorder. This confirms that the way in which the percolation structure develops and the scaling properties associated with this feature are those discussed in the previous section regarding the clean case and are largely independent of the presence of disorder.

Finally, we arrive at the same conclusion by considering the winding angle. This quantity is shown in Fig. 6, where the clean system and different disordered cases are shown. As in Fig. 4, the comparison is made by choosing times so as to have the same $R(t)$. Also in this case one observes an excellent superposition of all curves, further supporting the conclusion that the presence of disorder does not modify the percolative properties observed in the clean case. As a by-product, this also means that a scaling plot like the one presented in Fig. 7 for the pure case would look the same if data for the disordered models were used. This implies that the scaling properties discussed in the previous section for the winding angle apply in the presence of quenched disorder as well. A similar comparison between the connectedness function under weak and no disorder leads to the same conclusion.

As a final important point, let us discuss the role of the crossover time at which the growth law turns to a logarithmic form. As we said at the beginning of this section, our simulations do not even approach times of the order $t_{\rm cross}$. However, the existence of this crossover time is associated with a further characteristic length $\lambda(\epsilon) = R(t_{\rm cross})$ that might be relevant to the scaling properties discussed in Sec. III A. Indeed, considering, for example, the connectedness function, the dependence on $\lambda$ is expected to enter a scaling form in the following way:

$$C(r,t) = c\left(\frac{r}{R(t)}, \frac{L}{R_p(t)}, \frac{R(t)}{\lambda(\epsilon)}\right), \tag{26}$$

where for simplicity we use the same symbol $c$ for this three-entry scaling function. Clearly, since in the range of times considered in our simulations we have $t \ll t_{\rm cross}$ and consequently $R(t) \ll \lambda(\epsilon)$, the last entry in the above equation is always close to zero and can be neglected. This in turn makes our results independent of disorder $\epsilon$, a fact that has been called superuniversality [54]. Notice that this does not mean that disorder is ineffective, since the growth law $R(t)$ changes dramatically due to the quenched randomness. However, it is quite natural to expect that the insensitivity of $c$ on $\epsilon$ could be spoiled if times were pushed to sufficiently late regimes such that $R(t) \gtrsim \lambda(\epsilon)$. In this extremely-long-limit regime, the last entry in Eq. (26) could start, in principle, to play a role, introducing an $\epsilon$ dependence and spoiling the superuniversality. The investigation of such a very late regime requires a huge numerical effort that is beyond the scope of this paper and remains a challenge for future research.

## IV. CONCLUSION

In this paper we investigated the relevance of percolative effects on the phase-ordering kinetics of the two-dimensional Ising model quenched from the disordered phase to a very low final temperature. We considered the clean case as a benchmark and two forms of quenched randomness, random bonds and random fields. The presence and the properties of the percolation cluster are established using quantities such as the pair connectedness, which are efficient tools to detect the percolating wrapping structure hidden in the patchwork of growing domains.

In the first part of the paper we confirmed that the clean model with Glauber dynamics approaches critical percolation by using the following observables: the winding angle and the pair connectedness. The main finding of this paper is that the addition of weak quenched randomness, while sensibly changing the speed of the ordering process, does not impede the occurrence of critical percolation, nor does it change the way in which it sets in, even at a quantitative level. Indeed, we find that quantities such as the wrapping probabilities, the connectivity function, and the winding angle behave in the same way with great accuracy for any choice of the disorder strength, including the clean case, once time has been measured in units of the size $R(t)$ of the ordered regions.

This phenomenon can be accounted for in a scaling framework where coarsening, percolation, and disorder are associated with three characteristic lengths $R$, $R_p$, and $\lambda$, respectively. The interplay between them depends on the comparison between all these lengths, including the linear system size.

The results in [48] and in this paper show that the relevance of percolation, which was previously pointed out for two-dimensional clean systems, extends to the much less understood realm of disordered systems, making this issue of a quite general character. This not only opens the way for further studies on more general disordered systems (for instance, randomly diluted models where a more complex scaling structure was recently observed [45]), but also prompts the attention to a possible generalization of analytical theories where the properties of phase ordering are traced back to percolation effects, originally developed for clean systems, for the disordered cases.

**ACKNOWLEDGMENTS**

F.C. and F.I. thank the LPTHE Jussieu for hospitality during the preparation of this work. L.F.C. acknowledges support as a member of Institut Universitaire de France and thanks the KITP University of California at Santa Barbara for hospitality. This research was supported in part by the National Science Foundation under Grant No. PHY11-25915.

[1] A. J. Bray, Adv. Phys. **43**, 357 (1994).
[2] *Kinetics of Phase Transitions*, edited by S. Puri and V. Wadhawan (CRC, Boca Raton, 2009).
[3] J. J. Arenzon, A. J. Bray, L. F. Cugliandolo, and A. Sicilia, Phys. Rev. Lett. **98**, 145701 (2007).
[4] A. Sicilia, J. J. Arenzon, A. J. Bray, and L. F. Cugliandolo, Phys. Rev. E **76**, 061116 (2007).
[5] A. Sicilia, Y. Sarrazin, J. J. Arenzon, A. J. Bray, and L. F. Cugliandolo, Phys. Rev. E **80**, 031121 (2009).
[6] K. Barros, P. L. Krapivsky, and S. Redner, Phys. Rev. E **80**, 040101 (2009).
[7] J. Olejarz, P. L. Krapivsky, and S. Redner, Phys. Rev. Lett. **109**, 195702 (2012).
[8] T. Blanchard and M. Picco, Phys. Rev. E **88**, 032131 (2013).
[9] T. Blanchard, F. Corberi, L. F. Cugliandolo, and M. Picco, Europhys. Lett. **106**, 66001 (2014).
[10] D. Stauffer and A. Aharony, *Introduction to Percolation Theory* (Taylor and Francis, London, 1994).
[11] K. Christensen, *Percolation Theory* (Imperial College Press, London, 2002).
[12] A. A. Saberi, Phys. Rep. **578**, 1 (2015).
[13] T. Blanchard, L. F. Cugliandolo, M. Picco, and A. Tartaglia (unpublished).
[14] J. Cardy and R. M. Ziff, J. Stat. Phys. **110**, 1 (2003).
[15] F. Corberi, C. R. Phys. **16**, 332 (2015).
[16] V. Likodimos, M. Labardi, and M. Allegrini, Phys. Rev. B **61**, 14440 (2000).
[17] V. Likodimos, M. Labardi, X. K. Orlik, L. Pardi, M. Allegrini, S. Emonin, and O. Marti, Phys. Rev. B **63**, 064104 (2001).
[18] H. Ikeda, Y. Endoh, and S. Itoh, Phys. Rev. Lett. **64**, 1266 (1990).
[19] A. G. Schins, A. F. M. Arts, and H. W. de Wijn, Phys. Rev. Lett. **70**, 2340 (1993).
[20] D. K. Shenoy, J. V. Selinger, K. A. Grüneberg, J. Naciri, and R. Shashidhar, Phys. Rev. Lett. **82**, 1716 (1999).
[21] D. S. Fisher, P. Le Doussal, and C. Monthus, Phys. Rev. Lett. **80**, 3539 (1998).
[22] D. S. Fisher, P. Le Doussal, and C. Monthus, Phys. Rev. E **64**, 066107 (2001).
[23] F. Corberi, A. de Candia, E. Lippiello, and M. Zannetti, Phys. Rev. E **65**, 046114 (2002).
[24] M. Rao and A. Chakrabarti, Phys. Rev. E **48**, R25(R) (1993).
[25] M. Rao and A. Chakrabarti, Phys. Rev. Lett. **71**, 3501 (1993).
[26] C. Aron, C. Chamon, L. F. Cugliandolo, and M. Picco, J. Stat. Mech. (2008) P05016.
[27] F. Corberi, E. Lippiello, A. Mukherjee, S. Puri, and M. Zannetti, Phys. Rev. E **85**, 021141 (2012).
[28] S. Puri and N. Parekh, J. Phys. A **26**, 2777 (1993).
[29] E. Oguz, A. Chakrabarti, R. Toral, and J. D. Gunton, Phys. Rev. B **42**, 704 (1990).
[30] E. Oguz, J. Phys. A **27**, 2985 (1994).
[31] R. Paul, S. Puri, and H. Rieger, Europhys. Lett. **68**, 881 (2004).
[32] R. Paul, S. Puri, and H. Rieger, Phys. Rev. E **71**, 061109 (2005).
[33] R. Paul, G. Schehr, and H. Rieger, Phys. Rev. E **75**, 030104(R) (2007).
[34] F. Corberi, E. Lippiello, A. Mukherjee, S. Puri, and M. Zannetti, J. Stat. Mech. (2011) P03016.
[35] M. Henkel and M. Pleimling, Europhys. Lett. **76**, 561 (2006).
[36] M. Henkel and M. Pleimling, Phys. Rev. B **78**, 224419 (2008).
[37] J. H. Oh and D.-I. Choi, Phys. Rev. B **33**, 3448 (1986).
[38] F. Corberi, M. Zannetti, E. Lippiello, R. Burioni, and A. Vezzani, Phys. Rev. E **91**, 062122 (2015).
[39] M. F. Gyure, S. T. Harrington, R. Strilka, and H. E. Stanley, Phys. Rev. E **52**, 4632 (1995).
[40] S. Puri, D. Chowdhury, and N. Parekh, J. Phys. A **24**, L1087 (1991).
[41] S. Puri and N. Parekh, J. Phys. A **25**, 4127 (1992).
[42] A. J. Bray and K. Humayun, J. Phys. A **24**, L1185 (1991).
[43] B. Biswal, S. Puri, and D. Chowdhury, Physica A **229**, 72 (1996).
[44] H. Park and M. Pleimling, Phys. Rev. B **82**, 144406 (2010).
[45] F. Corberi, E. Lippiello, A. Mukherjee, S. Puri, and M. Zannetti, Phys. Rev. E **88**, 042129 (2013).
[46] C. Castellano, F. Corberi, U. M. B. Marconi, and A. Petri, J. Phys. IV **8**, 93 (1998).
[47] F. Corberi, E. Lippiello, and M. Zannetti, J. Stat. Mech. (2015) P10001.
[48] A. Sicilia, J. J. Arenzon, A. J. Bray, and L. F. Cugliandolo, Europhys. Lett. **82**, 10001 (2008).
[49] Y. Imry and S.-k. Ma, Phys. Rev. Lett. **35**, 1399 (1975).
[50] B. Duplantier and H. Saleur, Phys. Rev. Lett. **60**, 2343 (1988).
[51] B. Wieland and D. B. Wilson, Phys. Rev. E **68**, 056101 (2003).
[52] H. Pinson, J. Stat. Phys. **75**, 1167 (1994).
[53] J. L. Iguain, S. Bustingorry, A. B. Kolton, and L. F. Cugliandolo, Phys. Rev. B **80**, 094201 (2009).
[54] D. S. Fisher and D. A. Huse, Phys. Rev. B **38**, 373 (1988).